journal of the mechanical behavior of biomedical materials 135 (2022) 105432

Contents lists available at ScienceDirect

Journal of the Mechanical Behavior of Biomedical Materials

journal homepage: www.elsevier.com/locate/jmbbm

Critical size of kidney stone through ureter: A mechanical analysis

Yonggang Liu [a,b], Moxiao Li [a,b], Lusheng Qiang [a,b], Xuechao Sun [a,b], Shaobao Liu [a,b,*], Tian Jian Lu [a,b,**]

[a] State Key Laboratory of Mechanics and Control of Mechanical Structures, Nanjing University of Aeronautics and Astronautics, Nanjing, 210016, PR China
[b] MIIT Key Laboratory of Multifunctional Lightweight Materials and Structures, Nanjing University of Aeronautics and Astronautics, Nanjing, 210016, PR China

ARTICLE INFO

Keywords:
Blockage
Stone-ureter interaction
Urine pressure
Fung-type model
Finite element (FE)

ABSTRACT

Blockage of ureter caused by kidney stone, accompanied by severe pain/infections, is a high incidence urinary tract disease that has received extensive attention. Currently, in clinics, a kidney stone with diameter less than ~5 mm is considered capable of passing through ureter. However, this critical size (~5 mm) is empirically based, lacking quantitative analysis. In this study, we proposed a stone-ureter interaction model to quantificationally estimate the critical size of kidney stone passing through ureter. We revealed that the critical size of kidney stone is related to ureter size, about 11%–22% larger than the inner diameter of ureter. Further, based upon the Winkler elastic foundation beam model, we developed a simplified stone-ureter interaction model to evaluate how this critical size is dependent upon the stiffness of ureter and the surface roughness of kidney stone. The proposed model may help urologists improve the accuracy of personalized diagnosis and treatment.

1. Introduction

As a highly prevalent urological disorder (Alelign and Petros, 2018), kidney stones have long plagued humans with 12% incidence rate (López and Hoppe, 2010; Chauhan et al., 2009). Most kidney stones in human body can migrate to ureter along with urine. When a relatively large stone is passing through the ureter, the interaction between ureteral wall and stone usually triggers pain. More severely, a sufficiently large stone can block the pathway of urinary flow, causing backflow of urine (Najafi et al., 2016) and consequent complications such as urinary tract infections (Arant, 1991). Existing therapies for stone removing with regard to different situations mainly include: expulsive medical therapy (EMT) to facilitate stone passage, analgesics with extracorporeal shock wave lithotripsy, ureteroscopic lithotripsy, and laparoscopic ureterolithotomy (Song et al., 2010; Preminger et al., 2007). Typically, urologists choose a specific therapy according to the location, size, and shape of kidney stones (Song et al., 2010).

Based upon clinical statistical methodology, current guidelines of therapies empirically recommend that smaller stones with diameter less than ~5 mm can pass through ureter, while larger stones may need certain clinical therapies (Preminger et al., 2007; Segura et al., 1997; Mokhless et al., 2012; Jendeberg et al., 2017). Such guidelines, however, lack substantial physics principles, and may expose the patients to potential risks (Jendeberg et al., 2017). Specifically, there is no quantitative criterion to judge under what conditions a kidney stone can pass through ureter, and how geometrical and material parameters of stone and ureter affect the passage of stone. Therefore, to improve therapy accuracy and reduce potential risks, performing mechanical analysis is indispensable to determine the size range of kidney stones that can pass through ureter.

Given that ureter is the primary channel for transporting kidney stones to the outside of human body, the mechanical properties of ureter play a key role in determining the critical size of stone passing through it. By investigating ureter segments of mammals (*e.g.*, rabbit, dog, pig, and human foetus), it was found that ureter is typically a thick-walled tubular structure, exhibiting nonlinear, anisotropic, and pseudo-elastic response over finite strain (Yin and Fung, 1971). The ureter of rabbit displays nonlinear anisotropic mechanical response during *in vitro* inflation/extension testing, which can be well characterized using the four-parameter Fung-type strain energy function (Sokolis, 2011, 2014), called herein as the Fung-type model. Focusing upon human ureter under biaxial tension, Rassoli et al. (2014) characterized the mechanical

* Corresponding author. State Key Laboratory of Mechanics and Control of Mechanical Structures, Nanjing University of Aeronautics and Astronautics, Nanjing, 210016, PR China.
** Corresponding author. State Key Laboratory of Mechanics and Control of Mechanical Structures, Nanjing University of Aeronautics and Astronautics, Nanjing, 210016, PR China.
E-mail addresses: sbliu@nuaa.edu.cn (S. Liu), tjlu@nuaa.edu.cn (T.J. Lu).

https://doi.org/10.1016/j.jmbbm.2022.105432
Received 25 February 2022; Received in revised form 20 August 2022; Accepted 26 August 2022
Available online 2 September 2022

behavior of ureter using the Fung-type model, and concluded that ureter tissues exhibit anisotropy between longitudinal direction and circumferential direction. In the present study, the Fung-type model is also employed to characterize the deformation of human ureter caused by kidney stone.

This study aims to establish a mechanical model to calculate the critical size of kidney stone passing through ureter. Both theoretical analysis and numerical simulations with the finite element method (FEM) are employed to establish the mechanical model. To validate the proposed model, *in vitro* experiments are carried out. Critical urine pressure impelling a kidney stone to move within ureter is obtained for selected sizes of stone and ureter, from which the critical size of stone passing through ureter is determined based on human bearable maximum urine pressure.

2. Material and methods

2.1. Mechanical model of stone-ureter interaction

Adult human ureter is a highly flexible lumen (Woodburne and Lapides, 1972; Hanna et al., 1976), with a diameter ranging 4–6 mm and a length ranging 25–30 cm (Sokolis et al., 2017) (Fig. 1a). In accordance with previous studies (Vahidi et al., 2011; Vahidi and Fatouraee, 2012; Takaddus et al., 2018; Takaddus and Chandy, 2018), we simplify human ureter as a uniform axisymmetric tube such that a mechanical model can be established (Fig. 1b). When kidney stones migrate from kidney to ureter, small stones can pass through ureter along with urine (Chrispell and Fauci, 2011), while larger ones with size exceeding the inner diameter of ureter would be stuck in it (Fig. 1a). In our model, a sufficiently large kidney stone is considered as a rigid sphere to analyze the force state of the stone stuck in ureter. On the one hand, the resistance force (F_{re}) existing between the stone and ureter would hinder the stone from moving. On the other hand, the urine pressure (P_u) acting on the stone, which generates the driving force (F_{dr}) on the stone, would impel the stone to move in the blocked ureter. According to Newton's second law, the critical condition for kidney stone moving in ureter can be obtained as:

$$F_{re} = F_{dr} \tag{1}$$

with the effective area that urine pressure acts on the stone denoted as A_{eff}, the driving force can be expressed as $F_{dr} = P_u \cdot A_{eff}$, yielding:

$$F_{re} = P_u \cdot A_{eff} \tag{2}$$

The critical urine pressure (P_{ucr}) impelling a kidney stone to move, which we aim at, can be obtained by solving Eq. (2).

To solve Eq. (2), we introduce an intermediate variable, as follows. Firstly, for clarity, we define two states of ureter as shown in Fig. 1b: (1) initial state: a stone stuck in ureter without pressure P_u (*i.e.*, $P_u = 0$, dashed-line); (2) current state: a stone stuck in ureter with P_u (*i.e.*, $P_u > 0$, solid-line). To conveniently express the deformation and stress state in ureter wall, the polar coordinates (r, θ) are set up as shown in Fig. 1b. In initial state, there exists a non-contacting arc between ureter and stone with a separation angle $\theta = \alpha$ (Fig. 1b). Then, with the increase of P_u (*i.e.*, in current state), α would also increase due to expansion of ureter caused by P_u. Meanwhile, the effective area A_{eff} on the spherical stone (radius R_s) can be determined as $A_{eff} = \pi(R_s sin\alpha)^2$. On the other aspect, when the stone tends to move, the compression stress acting on stone-ureter interface, *i.e.*, $\sigma_{r(r=R_s)}$, yields a friction force f generated on the interface according to Coulomb's law of friction (Popov, 2017); Fig. 1d. With the increase of α, both the compression stress $\sigma_{r(r=R_s)}$ and the friction force f would hinder stone movement (see Fig. S1). Summation of $\sigma_{r(r=R_s)}$ and f on the stone then yields the resistance force F_{re}. Therefore, P_u, A_{eff} and F_{re} are all dependent upon the intermediate variable α, as:

$$\begin{cases} P_u = P_u(\alpha) \\ A_{eff} = \pi(R_s sin\alpha)^2 \\ F_{re} = F_{re}(\alpha) \end{cases} \tag{3}$$

A critical separation angle α_{cr} can thence be determined, as:

$$F_{re}(\alpha_{cr}) = P_u(\alpha_{cr}) \cdot \pi(R_s sin\alpha_{cr})^2 \tag{4}$$

Finally, the critical urine pressure P_{ucr} for a kidney stone to move in blocked ureter could be determined as $P_{ucr} = P_u(\alpha_{cr})$.

2.1.1. Relation between resistance force and separation angle

To determine the relation between resistance force F_{re} and separation angle α, the stone is taken as fixed when urine pressure P_u gradually increases from initial state of $P_u = 0$. In initial state, the ultimate separation angle could be determined as $\alpha_u = \pi - \alpha_0$ (Fig. 1b), α_0 being the initial separation angle. Supposing the separation angle reaches a certain value of $\alpha \in [\alpha_0, \pi - \alpha_0]$, we denote the compression stress

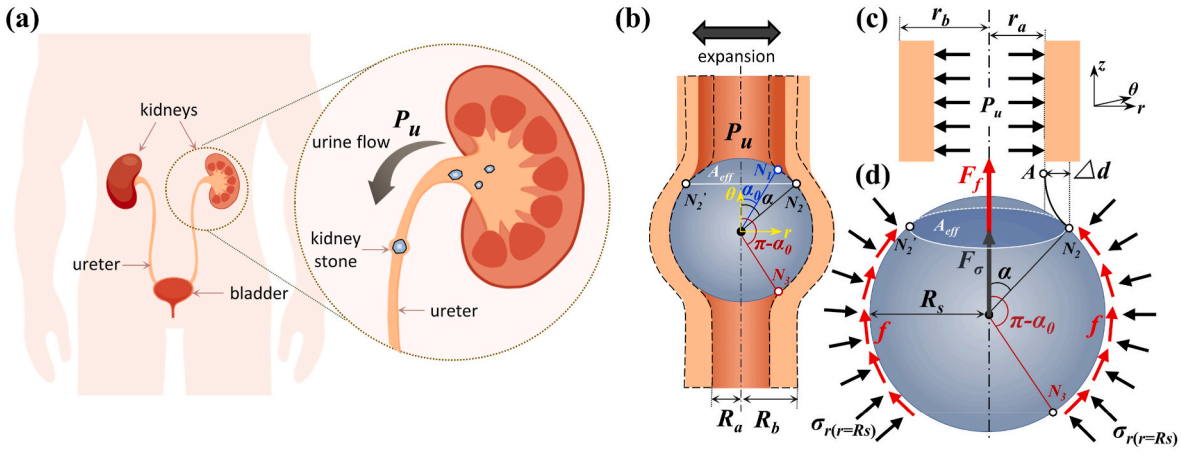

Fig. 1. Schematic of kidney stone-blocked ureter in human body and the mechanical modeling for stone-blocked ureter. **(a)** Kidney stone-blocked ureter: urine flow is cut off by kidney stone, leading to urine accumulation and increasing urine pressure (P_u). **(b)** Stone-ureter interaction model before (initial state marked with dashed line) and after deformation (current state marked with solid line) with urine pressure P_u. In initial state, ureter has inner radius R_a and outer radius R_b. Half central angle of non-contact arc between ureter and stone (defined as separation angle) in initial state is α_0. After deformation, the separation angle becomes α, and the effective area of P_u applied on stone is A_{eff}. The ultimate separation angle is π-α_0. **(c)** Deformation of ureter segment faraway from stone, with inner and outer radius after deformation (in current state) r_a and r_b. **(d)** Force state of stone caused by ureter. The stone is subjected to radial compression stress $\sigma_{r(r=Rs)}$ and friction force f caused by $\sigma_{r(r=Rs)}$. Vertical force components of $\sigma_{r(r=Rs)}$ and f on stone are F_σ and F_f.

within the unseparated region in initial state as $\sigma^0_{r(r=R_s)}(\theta)$, with $\theta \in [\alpha, \pi-\alpha_0]$. In current state, with an identical separation angle $\alpha \in [\alpha_0, \pi-\alpha_0]$ under $P_u > 0$, the compression stress within the unseparated region can be proved as $\sigma_{r(r=R_s)}(\theta) \approx \sigma^0_{r(r=R_s)}(\theta)$ in contact region $\theta \in [\alpha, \pi-\alpha_0]$; ***Supporting Information (SI) Section 2***. This conclusion enables simplifying the calculation of F_{re}, with arbitrary separation angle $\alpha \in [\alpha_0, \pi-\alpha_0]$, compression stress $\sigma_{r(r=R_s)}(\theta)$ in current state can be directly replaced by $\sigma^0_{r(r=R_s)}(\theta)$ in initial state, with $\theta \in [\alpha, \pi-\alpha_0]$. Therefore, the force component F_σ of $\sigma_{r(r=R_s)}$ on stone along the length direction of ureter (Fig. 1d) can be obtained as (***SI Section 1***):

$$F_\sigma(\alpha) = \pi R_s^2 \int_\alpha^{\pi-\alpha_0} \sigma^0_{r(r=R_s)}(\theta) sin2\theta d\theta,\ \alpha \in [\alpha_0, \pi-\alpha_0] \tag{5}$$

Similarly, the force component F_f of f on stone along the length direction of ureter (Fig. 1d) can be expressed as (***SI Section 1***):

$$F_f(\alpha) = 2\pi\mu_f R_s^2 \int_\alpha^{\pi-\alpha_0} \sigma^0_{r(r=R_s)}(\theta) sin^2\theta d\theta,\ \alpha \in [\alpha_0, \pi-\alpha_0] \tag{6}$$

where μ_f is the coefficient of static friction between ureter and stone. Finally, the relation between resistance force F_{re} on stone and separation angle α is given by:

$$F_{re}(\alpha) = F_\sigma(\alpha) + F_f(\alpha) \tag{7}$$

In the present study, to determine the specific value of $F_{re}(\alpha)$, the unknown quantities α_0 and $\sigma^0_{r(r=R_s)}(\theta)$ in Eqs. (5) and (6) are obtained using numerical methods.

Although $\sigma^0_{r(r=R_s)}$ cannot be obtained analytically, we note that $\sigma^0_{r(r=R_s)}$ is actually determined by the mechanical properties of ureter (denoted here as C_m), the size of ureter (inner radius R_a and outer radius R_b), and the radius of stone (R_s). Therefore, based on dimensional analysis, $\sigma^0_{r(r=R_s)}(\theta)$ can be expressed as $\sigma^0_{r(r=R_s)}(\theta) = f_1\left(C_m, \frac{R_b}{R_a}, \frac{R_s}{R_a}, \theta\right)$. Substituting $\sigma^0_{r(r=R_s)}(\theta)$ into Eqs. (5) and (6) yields:

$$F_{re}(\alpha) = \pi R_s^2 \cdot f_2\left(C_m, \mu_f, \frac{R_b}{R_a}, \frac{R_s}{R_a}, \alpha\right),\ \alpha \in [\alpha_0, \pi-\alpha_0] \tag{8}$$

2.1.2. Relation between urine pressure and separation angle

According to the Saint Venant principle (Timoshenko and Goodier, 1970), the deformation of a ureter segment faraway from a kidney stone is not affected by the stone but caused only by urine pressure P_u. As a result, the axisymmetric plane strain model holds for this faraway ureter segment (Fig. 1c). In cylindrical coordinates (r, θ) in cross section of ureter as shown in Fig. 1c, the mechanical equilibrium for the faraway ureter then requires:

$$\frac{d\sigma_r}{dr} + \frac{1}{r}(\sigma_r - \sigma_\theta) = 0 \tag{9}$$

where σ_r and σ_θ are the Cauchy stresses along radial and circumferential directions in ureter wall. The urine pressure P_u can be obtained by integrating Eq. (9) from inner radius r_a to outer radius r_b of ureter in current state (Ma et al., 2018).

Generally speaking, in initial state, a pressure P_{out} exists on the outside of ureter due to the confining effects on ureter caused by surrounding tissues. Therefore, in current state, the pressure p_{out} outside the ureter could be calculated as (Chandrasekharaiah and Debnath, 1994):

$$p_{out} = \frac{R_b}{r_b} P_{out} \tag{10}$$

where R_b is the outer radius of ureter in initial state. Combined with p_{out}, the urine pressure P_u is calculated as:

$$P_u - p_{out} = \int_{-P_u}^{-p_{out}} d\sigma_r = \int_{r_a}^{r_b} \frac{1}{r}(\sigma_\theta - \sigma_r) dr \tag{11}$$

Substituting Eq. (10) into Eq. (11) yields:

$$P_u = \int_{r_a}^{r_b} \frac{1}{r}(\sigma_\theta - \sigma_r) dr + \frac{R_b}{r_b} \cdot P_{out} \tag{12}$$

This equation, together with the constitutive model of ureter, provides the relation between P_u and inner radius r_a for faraway ureter, *i.e.*, $P_u(r_a)$.

To determine $P_u(\alpha)$, the relation between r_a and separation angle α, *i.e.*, $r_a(\alpha)$, should be also given. According to algebraic geometry (Fig. 1d), a relation between r_a and α could be established as:

$$r_a = R_s \cdot sin\alpha - \Delta d \tag{13}$$

where Δd is mathematically expressed as a series based on $sin\ \alpha$, as:

$$\Delta d = \sum_{i=0}^{\infty} a_i (sin\ \alpha)^i \tag{14}$$

with $sin\ \alpha \le 1$ insured, the series is convergent, with the coefficients a_i determined by the geometrical parameters and constitutive model of ureter via data fitting. Substituting Eq. (14) into Eq. (13) yields $r_a(\alpha)$.

Particularly, the profile connecting the faraway ureter and stone should be tangent to the two junctions, A and N_2 in Fig. 1d. Consequently, based on the condition of junction A ($r_a = R_a$, $\alpha = \alpha_0$) in initial state and junction N_2 ($r_a = R_s$, $\alpha = \frac{\pi}{2}$) in current state with $\alpha = \frac{\pi}{2}$, a simple linear relation between r_a and $sin\ \alpha$ in Eqs. (13) and (14) could be obtained, as:

$$r_a = R_s \cdot sin\ \alpha + (sin\ \alpha - 1) \cdot \frac{R_a - R_s \cdot sin\ \alpha_0}{sin\ \alpha_0 - 1} \tag{15}$$

Equation (15), together with Eq. (12), gives the relation $P_u(\alpha)$.

Upon combining Eqs. (4), (7), (12) and (15), the critical urine pressure P_{ucr} impelling a stuck kidney stone to move in ureter could be obtained. In this study, P_{ucr} is separately determined with the Neo-Hookean model (Eq. (19)), which is validated by performing *in vitro* experiments, and with the Fung-type model (Eq. (21)).

Actually, based on dimensional analysis, P_u is dependent upon the mechanical properties of ureter (C_m), the size of ureter, the deformation of ureter wall, and P_{out}. That is, P_u can be expressed as $P_u = f_3\left(C_m, \frac{R_b}{R_a}, \frac{r_a}{R_a}, \frac{r_b}{R_b}, P_{out}\right)$. R_a and R_b are the inner radius and outer radius of ureter in initial state, while r_a and r_b are the inner radius and outer radius of ureter after deformation. According to Eq. (15), $\frac{r_a}{R_a}$ is dependent upon $\frac{R_s}{R_a}$ and α. With the incompressibility of ureter (Eq. (S9)) accounted for, it can be deduced that $\frac{r_b}{R_b}$ is dependent upon $\frac{R_s}{R_a}$ and $\frac{R_b}{R_a}$. Therefore, $P_u(\alpha)$ can be expressed as:

$$P_u(\alpha) = f_4\left(C_m, \frac{R_b}{R_a}, \frac{R_s}{R_a}, P_{out}, \alpha\right),\ \alpha \in [\alpha_0, \pi-\alpha_0] \tag{16}$$

which, together with Eqs. (4) and (8), yields:

$$P_{ucr} = f_5\left(C_m, \mu_f, \frac{R_b}{R_a}, \frac{R_s}{R_a}, P_{out}\right) \tag{17}$$

Thus, P_{ucr} is mainly determined by C_m, μ_f, $\frac{R_b}{R_a}$, $\frac{R_s}{R_a}$, and P_{out}. In order to measure P_{ucr}, we define $\eta = \frac{R_b}{R_a}$ and $\xi = \frac{R_s}{R_a}$ so that different combinations of η and ξ can be selected to conduct *in vitro* experiments, as detailed below.

2.2. In vitro experiments

An *in vitro* experimental system is developed to verify the critical pressure P_{ucr} predicted by the proposed stone-ureter interaction model; Fig. 2. Latex tubes (Fig. S3a) are used to simulate ureter while tungsten steel spheres (Fig. S3b) are employed to simulate kidney stones, for the hardness of kidney stone is much higher than that of ureter (Vahidi et al., 2011; Zhong et al., 1993). With the inner radius of latex tube purposely selected to be smaller than that of tungsten steel sphere, the sphere is pressed into the tube to simulate stone-blocked ureter. To simulate the confining pressure of ureter in human body, the blocked latex tube is immersed in a water reservoir. To simulate urine, water is filled in the blocked latex tube. Water pressure in the tube is controlled to stimulate urine pressure via a syringe and measured via a pressure gauge, the latter connected to the tube with a T-branch pipe. As the syringe is slowly pushed (10 mm/min), the sphere would move from rest only if the pressure in the tube reaches a critical value P_{ucr}. A digital video camera (FDR-AX45, Sony, Japan) is employed to record the process, so that P_{ucr} can be captured (***SI Section 3.2***).

Experiments are carried out under two different conditions: (1) the tube is exposed to air, and (2) the tube is immerged in water with a fixed hydrostatic pressure of $P_{out} = 5.4$ kPa (*i.e.*, the tube is located 540 mm below the water surface in reservoir, as shown in Fig. 2). The tube sizes are chosen as $\eta = 1.5,\ 1.57,\ 2$ (Fig. S3a). Spheres with sizes varying as $\xi = 1$–1.5 (Fig. S3b) are tested for each tube, so that different values of critical pressure P_{ucr} can be obtained.

2.3. Estimation of static friction coefficient between ureter and kidney stone

When the stone-ureter interaction model is applied to calculate the critical size of kidney stone through human ureter, the static friction coefficient μ_f between ureter and kidney stone needs to be known according to Eq. (17). Therefore, a sample of uric acid stone taken from human body (Fig. 3a and b, provided by Tianjin University of Traditional Chinese Medicine) is collected herein as a representative to estimate μ_f, although there are several types of kidney stones (Cruz-May et al., 2021). Because human ureter is a kind of elastomer compared with kidney stone, μ_f is mainly determined by the roughness of kidney stone surface (Popov, 2017). Hence, the surface topography of the uric acid stone is obtained (Fig. 3c) by scanning electron microscope (SEM) (MAIA3, Tescan, Czech Republic). It is found that the uric acid stone sample comprises of cubic crystals (Fig. 3a and **c**), and the average edge length of the cubic can be measured as $\sim 20\ \mu m$.

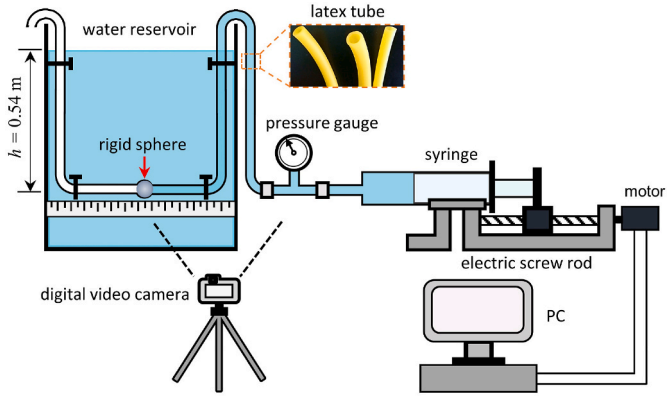

Fig. 2. Experimental setup of *in vitro* simulator for kidney stone passing through ureter. A tungsten steel sphere (red arrow) was put in a latex tube to simulate stone-blocked ureter, and the syringe was controlled by an electric screw rod connected to PC to manipulate inner pressure P_u in the blocked latex tube. A pressure gauge was used to measure the critical pressure P_{ucr} impelling the sphere to move in the tube. A digital video camera was employed to record the movement of sphere from rest and the change of pressure shown on pressure gauge.

To estimate μ_f, the SEM image of the kidney stone needs to be converted to surface profile. For brief herein, we choose six paths marked on the SEM image (Fig. 3c) to obtain surface profile. Since the crystal shape in SEM image is nearly cubic, the approximate maximum height of the surface profile is close to body diagonal of cubic crystal as $\sqrt{3} \times 20\ \mu m \approx 35\ \mu m$. Then, the surface profiles along the six paths can be obtained by linearly converting the gray value of SEM image to actual contour value of the kidney stone surface (Fig. 3d). Further, the average of the profiles is obtained as the black line shown in Fig. 3d.

Then, based on the average profile, the baseline of which is obtained based on the least square method as the red line shown in Fig. 3e, and the maximum tangent slope of the baseline is $tan|\theta_{0max}| = |k_{0max}| = 0.38$. Besides, the deviation with respect to the baseline of the average profile is accordingly obtained as the black line shown in Fig. 3f, and the baseline of the deviation is obtained as the red line. Similarly, the maximum tangent slope of the baseline of the deviation is $tan|\theta_{1max}| = |k_{1max}| = 0.12$. According to the friction theory (Popov, 2017), the static friction coefficient therefore can be estimated as:

$$\mu_f = tan(|\theta_{0max}| + |\theta_{1max}|) = \frac{|k_{0max}| + |k_{1max}|}{1 - |k_{0max}| \cdot |k_{1max}|} \approx 0.5 \tag{18}$$

2.4. FE analysis

2.4.1. FE modelling for in vitro experiments

As mentioned in **Section 2.1.1**, the initial separation angle α_0 and radial stress distribution $\sigma^0_{r(r=R_s)}(\theta)$ between the sphere and tube wall are difficult to obtain analytically. Therefore, a FE (finite element) model is developed in Abaqus (Version 2019; Dassault Systèmes simulia Corp., RI, USA) to calculate both α_0 and $\sigma^0_{r(r=R_s)}(\theta)$. The results enable determining the P_{ucr} theoretically based on the mechanical model of stone-ureter interaction, which is then compared with *in vitro* experimental measurement.

Since the geometrical characteristics of the sphere and tube are axisymmetric with regard to the center line of the tube, axisymmetric FE models are developed (Fig. 4a). Geometrical dimensions of the FE models are coincident with those of test samples used *in vitro* experiments, with $\eta = \frac{R_b}{R_a} = 1.5,\ 1.57,\ 2$ for the tubes (with inner radius R_a and outer radius R_b) and with $\xi = \frac{R_s}{R_a} = 1$–$1.5$ for the spheres (with radius R_s). The rectangular part represents the longitudinal section of the latex tube wall, the length of which is more than twice of the diameter of rigid sphere, so as to ensure that the upper and lower boundary constraints have no impacts on stress distribution in the latex tube caused by the sphere. The arc curve represents the boundary of the sphere.

For material properties, the Neo-Hookean hyperelastic model (Eq. (19)) with $C_{10} = 0.1465$ MPa (***SI Section 3.1.3***) is assigned to the latex tube, and the section property of analytical rigid body is assigned to the sphere for tungsten steel sphere is much stiffer than latex tube.

The 4-node bilinear axisymmetric quadrilateral, hybrid elements (CAX4RH) are employed to partition the latex tube, with a minimum element size of 1/1000 tube length to guarantee the convergence of FE results. Mesh partition, however, is not necessary for the sphere since it is assigned with the property of analytical rigid body.

The tube and sphere are assembled side by side with the edge of the sphere being tangent to the inner surface of tube wall. A contact property with the friction coefficient $\mu_f = 0.475$ (***SI Section 3.1.4***) is assigned to the surface pair of sphere and inner surface of tube along the tangent direction.

A displacement load $u_x = R_s - R_a$ along the x-axis applied on the sphere yields that the center of sphere would be finally coaxial with the center line of tube (Fig. 4b). The y-axisymmetric displacement constraints of $u_y = \omega_x = \omega_z = 0$ are applied on the upper and lower

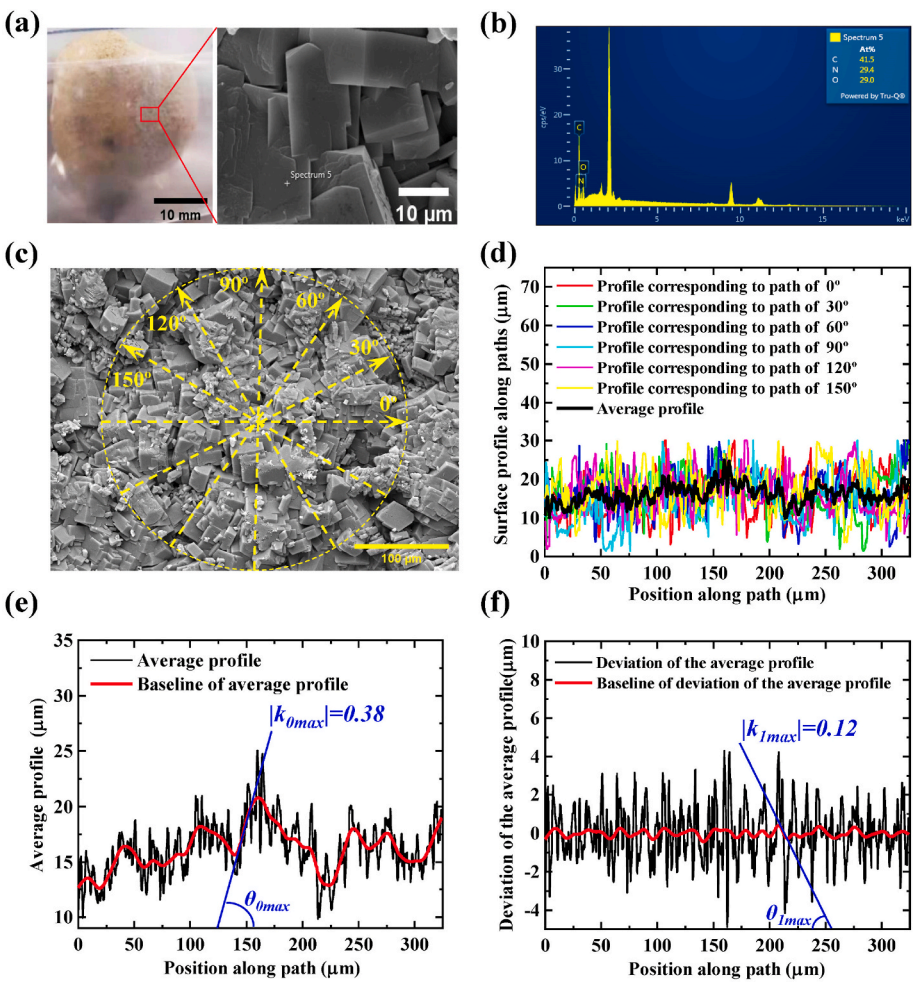

Fig. 3. Estimation of friction coefficient between kidney stone and ureter. **(a)** Image of kidney stone sample and elemental composition analysis for the stone sample. **(b)** Energy spectrum diagram of the stone sample, which shows that there are three main chemical elements of carbon, nitrogen, and oxygen, indicating that the sample is uric acid stone. **(c)** SEM image of the surface of the uric acid stone sample and the paths selected for obtaining the surface profile of the stone. **(d)** the surface profiles corresponding to the six paths. **(e)** the average of the surface profiles corresponding to the six paths. **(f)** the deviation with respect to the baseline of the average profile.

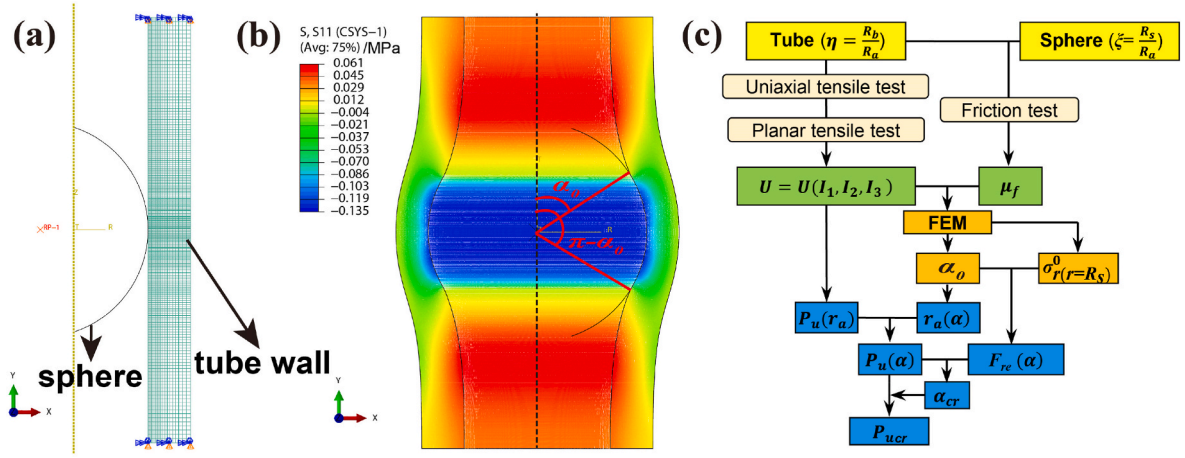

Fig. 4. FE (finite element) simulation for obtaining the stress distribution and deformation in latex tube caused by tungsten steel sphere. **(a)** FE model of tungsten steel sphere and latex tube; **(b)** compression stress distribution $\sigma^0_{r(r=R_s)}$ and deformation of latex tube based on FE simulation; and **(c)** flowchart for calculating the critical pressure P_{ucr} needed to move the sphere in tube.

boundaries of the tube to ensure that its deformation is *y*-axisymmetric. Further, for the tube immersed 540 mm underwater, not only the displacement loads but also the pressure ($P_{out} = 5.4\ kPa$) on the outer surface of the tube are applied to the FE model.

Finally, the initial separation angle α_0 and the compression stress $\sigma^0_{r(r=R_s)}$ can be determined from the FE results, as illustrated in Fig. 4b; correspondingly, the critical pressure P_{ucr} can be obtained theoretically based on the stone-ureter interaction model. The whole process is summarized as the flowchart of Fig. 4c.

2.4.2. FE modelling for human ureters

The wall thickness and inner radius of human ureter are not uniform

lengthwise (Hanna et al., 1976), varying with different individuals (Sokolis et al., 2017), and hence the ratio of ureter outer radius R_b to inner radius R_a (*i.e.*, $\eta = \frac{R_b}{R_a}$) is a variable. For illustration, we consider the upper limit η_{max} and the lower limit η_{min} for human ureter to calculate the critical size of kidney stone passing through it. Human ureter wall thickness was found to exhibit a negative linear relation with ureter inner radius (Sokolis et al., 2017). Consequently, the upper limit η_{max} may be determined by maximum wall thickness (~1.13 mm) and minimum inner radius (~0.47 mm), as $\eta_{max} = 3.40$. The lower limit η_{min} may be determined by minimum wall thickness (~0.52 mm) and maximum inner radius (~1.75 mm), as $\eta_{min} = 1.30$.

For the two limit conditions (*i.e.*, $\eta_{min} = 1.30$ and $\eta_{max} = 3.40$), FE models are separately developed (Fig. 5a and b). The kidney stone is modeled as a rigid sphere with radius varying as $R_s = R_a$–$1.3R_a$ (*i.e.*, $\xi = 1$–1.3). The static friction coefficient $\mu_f = 0.5$ obtained based on SEM images of uric acid stone (***Section 2.3***) is adopted, as the average friction coefficient between kidney stone and ureter. The Fung-type constitutive model (Eq. (21)) is assigned to the ureter, with relevant material constants selected as $C = 0.4056$ MPa, $a_{1111} = 0.7091$, $a_{2222} = 0.1856$ and $a_{1122} = 0.8892$ (Rassoli et al., 2014). The 4-node bilinear axisymmetric quadrilateral, hybrid elements (CAX4RH) are employed to partition the ureter wall, with a minimum element size of 1/2000 ureter length to guarantee the convergence of FE results. Displacement and load conditions are applied on each FE model in a way similar to the FE models of latex tube and tungsten steel sphere (***Section 2.4.1***). Numerical results obtained from the FE models are subsequently used to determine the initial separation angle α_0 and compression stress $\sigma^0_{r(r=R_s)}$ in Eqs. (5), (6) and (15). Finally, these results are used to theoretically calculate the critical pressure P_{ucr} (Fig. 4c).

3. Results

3.1. Verification of stone-ureter interaction model

To characterize the mechanical behavior of latex tubes used in the present mechanical tests (***SI Section 3.1***), the Neo-Hookean model is employed, given by:

$$U = C_{10}(I_1 - 3) \tag{19}$$

where U is the strain energy function, C_{10} is a material constant, $I_1 = \lambda_1^2 + \lambda_2^2 + \lambda_3^2$ is the first strain invariant, and $(\lambda_1, \lambda_2, \lambda_3)$ are the three principal stretch ratios. To simplify the calculation, the material of latex tubes is assumed incompressible, *i.e.*, $\lambda_1\lambda_2\lambda_3 = 1$. Combining Eqs. (12) and (19) leads to the relation between the pressure in latex tube P_u and the tube inner radius r_a in the current state, as (***SI Section 4***):

$$P_u = C_{10}\left(\frac{R_b^2}{r_a^2 + R_b^2 - R_a^2} - \frac{R_a^2}{r_a^2} + ln\frac{r_a^2}{R_a^2} - ln\frac{r_a^2 + R_b^2 - R_a^2}{R_b^2}\right) + P_{out}\frac{R_b}{\sqrt{r_a^2 + R_b^2 - R_a^2}} \tag{20}$$

where R_a and R_b are the inner radius and outer radius of latex tube in initial state, and P_{out} is the external pressure of latex tube. With Eq. (20) and the initial separation angle α_0 and compression stress $\sigma^0_{r(r=R_s)}$ obtained from FE simulation (Fig. 4b), critical pressure P_{ucr} can be theoretically determined as shown in flowchart Fig. 4c.

Fig. 6a and **b** displays both the theoretical and *in vitro* experimental results of P_{ucr} for different combinations of tube size (*i.e.*, $\eta = 1.5$, 1.57 and 2) and sphere size (*i.e.*, $\xi = 1$–1.5). The theoretically calculated critical pressure P_{ucr} of latex tube, either exposed to air or immersed under water, is seen to agree well with experimental data, thus validating the proposed stone-ureter interaction model.

3.2. Critical size of kidney stone passing through ureter

It has been demonstrated that the constitutive model of human ureter is given by the well-known four parameters Fung-type model, as:

$$U = \frac{C}{2}(e^Q - 1),\ Q = a_{1111}E_{\theta\theta}^2 + a_{2222}E_{zz}^2 + 2a_{1122}E_{\theta\theta}E_{zz} \tag{21}$$

where U is the strain energy function; C, a_{1111}, a_{2222} and a_{1122} are material constants; $E_{\theta\theta} = \frac{1}{2}(\lambda_\theta^2 - 1)$ and $E_{zz} = \frac{1}{2}(\lambda_z^2 - 1)$ are the Lagrange strains, with principal stretch ratios defined along circumferential and longitudinal directions. To simplify the calculation, the incompressibility of ureter (Sokolis, 2011) is hypothesized with $\lambda_r\lambda_\theta\lambda_z = 1$. Combining Eqs. (12) and (21) leads to the following relation between P_u and inner radius r_a of ureter in current state (***SI Section 5***):

$$P_u = \frac{1}{4}C\sqrt{\pi a_{1111}}\left\{erfi\left[\frac{\sqrt{a_{1111}}}{2}\left(\frac{r_a^2}{R_a^2} - 1\right)\right] - erfi\left[\frac{\sqrt{a_{1111}}}{2}\left(\frac{r_a^2}{R_a^2} - 1\right)\frac{R_a^2}{R_b^2}\right]\right\} + P_{out}\frac{R_b}{\sqrt{r_a^2 + R_b^2 - R_a^2}} \tag{22}$$

where *erfi* is the imaginary error function (Morris and Leach, 2015), and R_a and R_b are the inner radius and outer radius of ureter in initial state. Similarly, with Eq. (22) and the initial separation angle α_0 and compression stress $\sigma^0_{r(r=R_s)}$ obtained from FE simulation (Fig. 7), critical pressure P_{ucr} can be theoretically determined as shown in flowchart

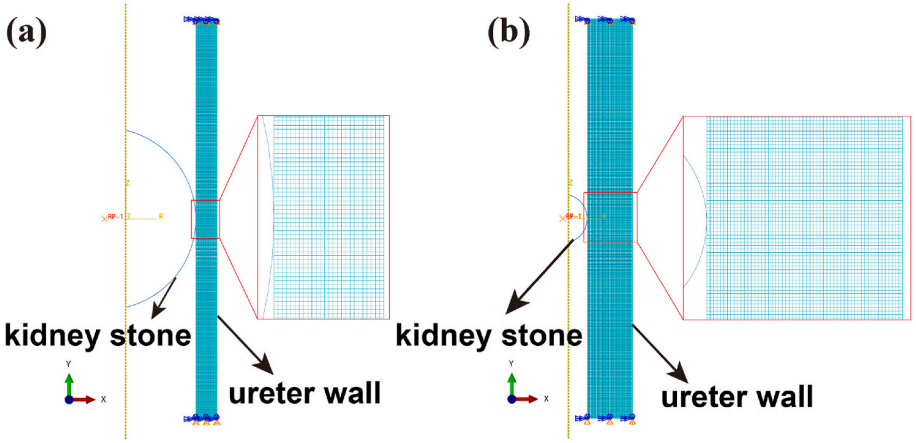

Fig. 5. FE simulation for stress distribution and deformation in ureter caused by a kidney stone: **(a)** FE model of kidney stone and ureter with $\eta = 1.3$, and **(b)** FE model of kidney stone and ureter with $\eta = 3.4$.

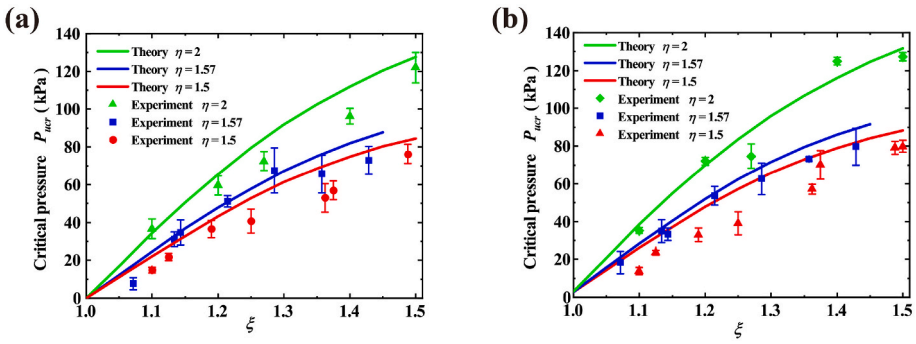

Fig. 6. (a) Critical pressures obtained based on FEM and experiment with the latex tube exposed to air, and **(b)** critical pressures obtained based on FEM and experiment with the latex tube immersed under water.

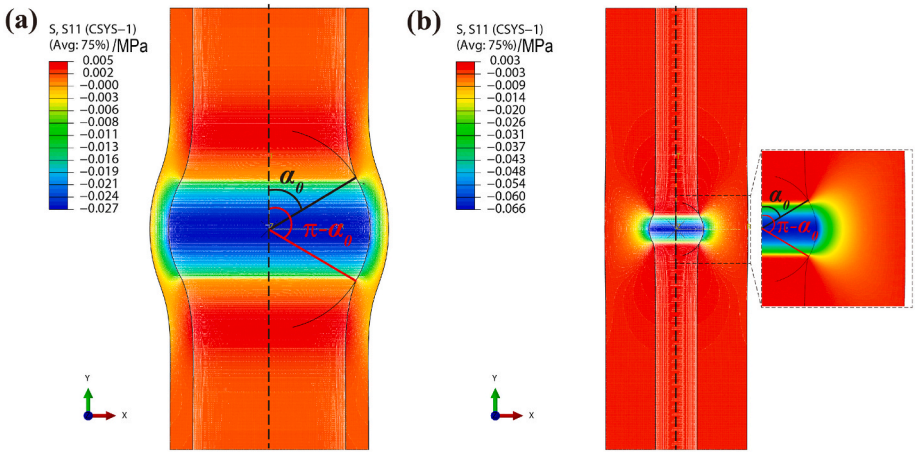

Fig. 7. (a) Compression stress distribution $\sigma^0_{r(r=R_s)}$ and deformation in ureter caused by kidney stone with $\eta = 1.3$. **(b)** Compression stress distribution $\sigma^0_{r(r=R_s)}$ and deformation of ureter caused by kidney stone with $\eta = 3.4$.

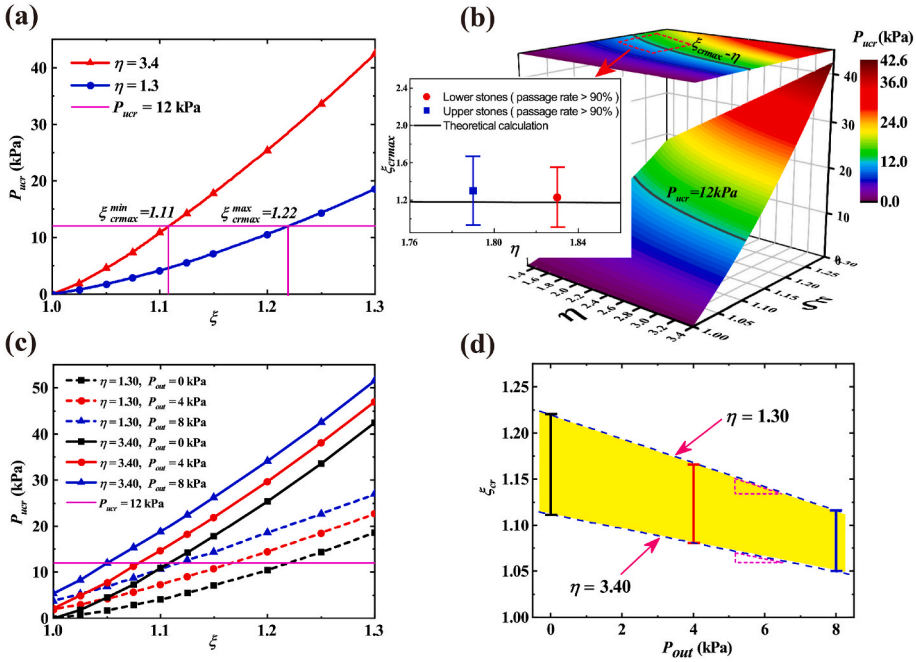

Fig. 8. (a) P_{ucr} versus ξ for $\eta_{max} = 3.4$ and $\eta_{min} = 1.3$; **(b)** P_{ucr} versus ξ and η, and comparison between clinical data and theoretical results for dimensionless critical size of kidney stone passing through ureter; **(c)** P_{ucr} versus ξ with different P_{out} (0 kPa, 4 kPa, 8 kPa) outside ureter for $\eta_{max} = 3.4$ and $\eta_{min} = 1.3$; **(d)** dimensionless critical size of stone (ξ_{cr}) versus P_{out}, with P_{ucr} = 12 kPa.

Fig. 4c.

Fig. 8a presents the critical pressure P_{ucr} for $\xi = 1$–1.3 (with $\eta_{min} = 1.30$ and $\eta_{max} = 3.40$). It is seen that P_{ucr} positively correlated with η and ξ, *i.e.*, thicker ureter wall and bigger kidney stone lead to larger P_{ucr}. Given that the physiological maximum urine pressure in human ureter is ~12 kPa (Schwalb et al., 1993), the range of maximum dimensionless size of kidney stone passing through ureter is determined as $\xi_{crmax}^{min} = 1.11$ to $\xi_{crmax}^{max} = 1.22$ (Fig. 8a). Therefore, the maximum critical diameter of kidney stone passing through ureter is calculated to be 11%–22% larger than the inner diameter of ureter. As a result, for human ureter with inner diameter varying from 0.94 mm to 3.5 mm (Sokolis et al., 2017), the maximum diameter of kidney stone varies from 1.04 mm to 4.27 mm. This reveals that the critical stone size (*i.e.*, the critical size of stone passing through ureter, same as below) is significantly influenced by ureter size.

Further, a three-dimensional graph of critical pressure $P_{ucr}(\xi, \eta)$ is obtained by linear interpolation with regard to η. Also, based on the maximum urine pressure of $P_{ucr} = 12$ kPa, how the maximum dimensionless critical stone size ξ_{crmax} varies with η, *i.e.*, the $\xi_{crmax} - \eta$ relation, is determined (black solid line in $\xi - \eta$ plane of Fig. 8b). To validate the stone-ureter interaction model, the values of η for upper and lower ureter (***SI Section 6***), together with stone sizes based on clinical statistics (***SI Section 6***) for upper and lower ureter (Jendeberg et al., 2017), are compared with the theoretical $\xi_{crmax} - \eta$ relation in Fig. 8b. The predicted $\xi_{crmax} - \eta$ relation agrees well with clinical statistic data.

Next, how the confining pressure P_{out} affects the critical stone size is investigated. For simplicity, the confining pressure is ideally deemed as hydrostatic pressure. Upon taking P_{out} sequentially as 0 kPa, 4 kPa and 8 kPa, it is found that compared with the state of $P_{out} = 0kPa$, the predicted P_{ucr} increases evenly with increment nearly equal to P_{out} (Fig. 8c). For illustration, based on $P_{ucr} = 12$ kPa, the dimensionless critical stone size ξ_{cr} (between $\eta = 1.30$ and $\eta = 3.40$) versus P_{out} relation, *i.e.*, the $\xi_{cr} - P_{out}$ relation, is determined (Fig. 8d). The upper boundary (with $\eta = 1.30$) and lower boundary (with $\eta = 3.40$) reveal that ξ_{cr} exhibits a negative linear relation with P_{out}, and the upper boundary has a slope larger than that of the lower boundary. That is, the smaller the ureter size ratio (η), the more obvious the effects of confining pressure on critical stone size.

3.3. Effects of ureter stiffness and surface roughness of stone on critical stone size

3.3.1. The stone-ureter interaction model based on elastic foundation beam model

As mentioned above, for human ureter, the value of η ranges from 1.3 to 3.4. When the ureter is thin-walled (*e.g.*, $\eta = 1.30$) and ξ is close to one, an analytical solution of P_{ucr} can be obtained by simplifying the stone-ureter interaction model as an elastic foundation beam model (EFBM).

When a thin-walled tube (*i.e.*, wall thickness $h \ll R_a$) deforms with the radial displacement of tube wall satisfying $\Delta r \ll R_a$ (Fig. 9a), small deformation hypothesis can be adopted to calculate the deformation. Since the tube wall thickness is small relative to tube radius, the tube is taken as composed of longitudinal 'fibers' and circumferential 'fibers'. The longitudinal 'fibers' play a role like beams mainly undertaking bending load, while the circumferential ones act as strings mainly undertaking stretching load. The latter equivalently prevents the former from deforming along the radial direction. Particularly, if the tube is made of a linear elastic material, the confining effect of circumferential 'fibers' on longitudinal 'fibers' can be regarded as elastic springs. The tube wall can thence be taken as equivalent to the superposition of longitudinal beam and springs (Fig. 9b), leading to the elastic foundation beam model (EFBM) or the Winkler elastic foundation model (Yankelevsky and Eisenberger, 1986). The equivalent stiffness coefficient of the springs (*i.e.*, foundation) is obtained as (***SI Section 7***):

$$k = \frac{hE_1}{R_a^2} \tag{23}$$

where E_1 is the Young's modulus of circumferential 'fibers'. Due to axial symmetry of the model, a longitudinal section of the tube with unit thickness is taken as EFBM to analyze the whole tube (Fig. 9b). With the deflection of tube wall caused by the size difference of tube and sphere

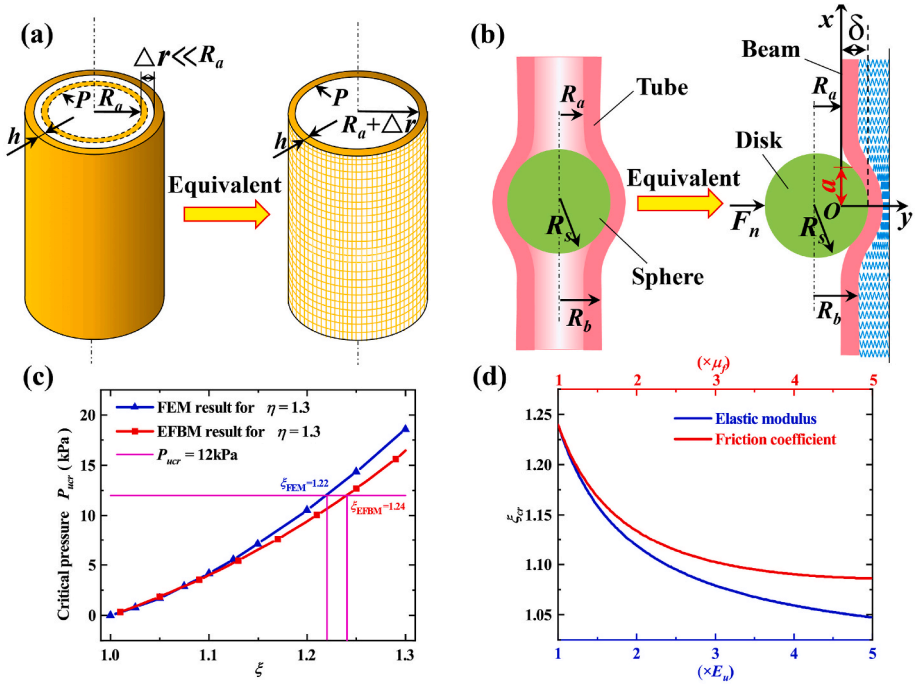

Fig. 9. Elastic foundation beam model is used to analyze thin-walled ureter: **(a)** deformation behavior of thin-walled tube, **(b)** equivalence of sphere-tube model to elastic foundation beam model, **(c)** comparison of critical pressures (P_{ucr}) calculated with FEM and elastic foundation beam model (EFBM) for $\eta = 1.3$, and **(d)** variation of dimensionless critical stone size (ξ_{cr}) for $\eta = 1.3$.

denoted by $\delta = R_s - R_a$, an equivalent concentrated load F_n applied on the longitudinal beam can be determined as (***SI Section 7***):

$$F_n = \frac{2k\delta}{\beta} \tag{24}$$

where $\beta = \sqrt[4]{\frac{3k}{E_2 h^3}}$ and E_2 is the Young's modulus of longitudinal 'fibers'.

Contact effect between the circular disk and beam (Fig. 9b) is considered in accordance with the classical Hertzian contact theory (Timoshenko and Goodier, 1970). The length of the half contact region caused by the equivalent concentrated load F_n between the disk and beam could be determined as:

$$a = \sqrt{\frac{4R_s F_n}{\pi E_2}} \tag{25}$$

Because the contact region is relatively small, the component of $\sigma_{r(r=R_s)}$ along the x-axis could be neglected. The resistance force F_{re} between the tube and sphere is thence calculated as (***SI Section 7***):

$$F_{re}(x) = F_f(x) = 4F_n\mu_f R_s\left[\frac{a-x}{2a}\sqrt{1-\left(\frac{a-x}{a}\right)^2}+\frac{1}{2}arcsin\left(\frac{a-x}{a}\right)+\frac{\pi}{4}\right] \tag{26}$$

where x is the abscissa of the separation region, and μ_f is the static friction coefficient between the sphere and tube.

Based on the EFBM, the inner pressure P_u correlated to current inner radius r_a of the tube can be determined as:

$$P_u = k\Delta r = k(r_a - R_a) \tag{27}$$

Also, the relation between r_a and x is obtained based on Eq. (15), as:

$$r_a = \sqrt{R_s^2-(a-x)^2}+\left[\sqrt{1-\left(\frac{a-x}{R_s}\right)^2}-1\right]\cdot\frac{R_a-\sqrt{R_s^2-a^2}}{\sqrt{1-\left(\frac{a}{R_s}\right)^2}-1} \tag{28}$$

Upon substituting Eq. (28) into Eq. (27), $P_u(x)$ can be determined. Finally, P_{ucr} is obtained by substituting the root of equation $P_u(x)\cdot\pi[R_s^2-(a-x)^2] = F_{re}(x)$ into $P_u(x)$.

Based on the EFBM and the Fung-type constitutive model, for the case of $\eta = 1.30$ and $\mu_f = 0.5$, P_{ucr} is calculated by taking the secant moduli along the circumferential and longitudinal directions of ureter as E_1 and E_2 (***SI Section 8***). Then, comparing the calculated P_{ucr} based on the EFBM and that calculated by the FEM indicates that the two results agree well within the interval of $\xi = 1$–1.3 (Fig. 9c). Thus, the EFBM is valid to analyze the ureter with $\eta = 1.30$. Correspondingly, the critical dimensionless stone size under $P_{ucr} = 12$ kPa is obtained based the EFBM as $\xi_{cr} = 1.24$, which is very close to that ($\xi_{cr} = 1.22$) calculated with the FEM.

3.3.2. Relation of critical stone size versus ureter stiffness and stone surface roughness

In clinic practice, the mechanical property of ureter such as ureter stiffness is often altered, *e.g.*, by medical expulsive therapy (MET), to facilitate the passage of kidney stone (Tzortzis et al., 2009). However, how the stiffness variation of ureter affects stone passage remains elusive. Further, there exist several different types of kidney stone (Cruz-May et al., 2021), which exhibit different surface roughness and hence would have different impacts on stone passage. These impacts are not easy to evaluate in clinic practice. Therefore, based on the EFBM, the effects of ureter stiffness (*i.e.*, elastic modulus) and kidney stone surface roughness (*i.e.*, friction coefficient) on critical stone size (*i.e.*, ξ_{cr}) are quantified, as illustrated below.

For $P_{ucr} = 12$ kPa and $\eta = 1.30$, Fig. 9d displays the predicted variation trend of ξ_{cr} with increasing elastic modulus E_u of ureter ($E_1 = 0.465$ MPa and $E_2 = 0.02$ MPa) or friction coefficient ($\mu_f = 0.5$). It can be seen that increasing either E_u or μ_f causes ξ_{cr} to decrease, finally reaching a constant. Softening the ureter would thus facilitate stone passage, and a smoother stone would pass through ureter more easily. Also, E_u has a more noticeable effect on ξ_{cr} compared with μ_f, indicating that the critical stone size is more sensitive to ureter stiffness than stone surface roughness.

4. Discussion

In clinical practice, numerous factors affect the passage of kidney stone. For instance, a strong correlation exists between the size/location of stone and the likelihood of stone passage (Ueno et al., 1977; Zhang and Steinberg, 2019). Other predictive factors, *e.g.*, C-reactive protein (CRP), hydronephrosis (Özcan et al., 2015; Ahmed et al., 2015; Aldaqadossi, 2013; Park et al., 2013; Goertz and Lotterman, 2010) and the sides of ureter the stone generated (Sfoungaristos et al., 2012), are also related to stone passage. These factors, however, are at present scattered and lack systematic investigations. From the view of mechanics, key factors affecting stone passage can be summarized based on our stone-ureter interaction model. The critical urine pressure P_{ucr} impelling a kidney stone to move can be deduced as Eq. (17). The stone could move through ureter only if the urine pressure P_u exceeds its critical value P_{ucr}. Therefore, it can be concluded that the mechanical factors affecting stone passage are the ones dictating P_{ucr}, including stone size (R_s), ureter size ($\frac{R_b}{R_a}$), stone surface roughness (μ_f), ureter stiffness (E_u), confining pressure (P_{out}), and urine pressure P_u. These factors would help urologists judging the possible aspects that could facilitate stone passage.

In addition, a variety of approaches have been developed to surgically manage kidney stones, including conservative approaches like medical expulsive therapy (MET), and invasive approaches such as shockwave lithotripsy (SWL), ureteroscopy (URS), and percutaneous nephrolithotomy (PCNL) (Zhang and Steinberg, 2019). For relatively small stones, the first approach is watchful waiting, with or without the accompanying MET (Preminger et al., 2007). However, the conservative approaches may make the patient endure symptoms to no benefit such as pain (Jendeberg et al., 2017; Miller and Kane, 1999), and may be associated with potential risks to renal function (Miller and Kane, 1999). In contrast, larger stones stuck in ureter are generally treated using invasive approaches. The major risk of invasive approaches is exposing the patient to potential complications such as anaesthesia, upper urinary tract infections, etc. (Jendeberg et al., 2017). The current therapy guidelines recommend MET for kidney stones with a diameter of 5–10 mm, and surgical removal for those larger than 10 mm (Preminger et al., 2007). Nevertheless, such guidelines may not be effective for all patient groups due to individual differences, causing potential risks for the patients. Therefore, it is necessary to establish a new criterion judging under what conditions a stone can pass through ureter for different individuals, so that appropriate treatment strategy would be selected to reduce the potential risks.

In clinics, the size and shape of kidney stone and the morphology of ureter can be determined using noninvasive imaging technologies, *e.g.*, abdominal ultrasonography, magnetic resonance urography (MRU) and computed tomography (CT) urography (Zhu et al., 2020; Mohammadinejad et al., 2021; Hosseini et al., 2018; Yoshida et al., 2017). Accordingly, the size ratio η of the normal ureter (without stone obstruction) and dimensionless size ξ of stone can also be determined by such noninvasive imaging technologies. Meanwhile, the inner radius (r_a) and outer radius (r_b) of stone-obstructed ureter can be determined analogously. Then, based on Eq. (22), the urine pressure P_u caused by stone can be calculated. Besides, based on Fig. 8b, the critical pressure P_{ucr} with regard to ξ and η can be determined. Given that the human bearable maximum urine pressure is about 12 kPa, when urine pressure P_u in human body satisfies $P_{ucr} < P_u < 12\ kPa$, a kidney stone is expected to pass through ureter. Otherwise, when P_{ucr} exceeds 12 kPa, the stone

cannot pass through ureter, thus suggesting surgical intervention. In clinical practice, this proposal would potentially become a new criterion to judge stone passage through ureter for different individuals, and prospectively ensure that patients receive evidence-based treatment.

It should be noted that our study only focuses on the ideal spherical stone, while the shapes of kidney stone in reality are complex, which can be categorized as either even or uneven (*e.g.*, jagged) (Cloutier et al., 2015). Most of the even stones are approximately ellipsoid-like (Reimer et al., 2020). Compared with ellipsoid-like stones, the adoption of spherical stone in this study would yield conservative conclusions for predicting the passage of even stone in ureter. For uneven stones, however, the sharp points on the jagged surface may easily cause high stress concentrations in ureter wall, making the ureter injured, which is different from our concern that the ureter should not be damaged during stone passage. Nonetheless, relative to even stones, the uneven stones raise a new and more complicated mechanical problem, which will be investigated in a future study, both experimentally and numerically.

In summary, our study provides a theoretical method to help urologists better understand how the passage of kidney stone through ureter is affected by relevant factors mentioned above, and potentially throw light on a new criterion to judge stone passage through ureter for different individuals.

5. Conclusions

A stone-ureter interaction model has been proposed to quantitatively estimate the critical size of kidney stones passing through ureter. It is demonstrated that the critical diameter of kidney stones is 11%–22% larger than the inner diameter of ureter, but negatively correlated to the confining pressure outside the ureter. For thin-walled ureter, an elastic foundation beam model (EFBM) has been developed to analyze how the elastic modulus of ureter and the friction coefficient between ureter and kidney stone influence the critical stone size. The proposed model may help urologists improve the accuracy of personalized diagnosis and treatment.

CRediT authorship contribution statement

Yonggang Liu: Writing – original draft, Formal analysis. **Moxiao Li:** Visualization, Data curation. **Lusheng Qiang:** Validation, Methodology. **Xuechao Sun:** Data curation. **Shaobao Liu:** Supervision, Funding acquisition, Conceptualization. **Tian Jian Lu:** Project administration, Funding acquisition, Conceptualization.

Declaration of competing interest

The authors declare that they have no known competing financial interests or personal relationships that could have appeared to influence the work reported in this paper.

Data availability

Data will be made available on request.

Acknowledgements

This work was financially supported by the National Natural Science Foundation of China (12032010 and 11902155), by the Natural Science Foundation of Jiangsu Province (BK20190382), by the foundation of Jiangsu Provincial Key Laboratory of Bionic Functional Materials, and by the Foundation for the Priority Academic Program Development of Jiangsu Higher Education Institutions.

Appendix A. Supplementary data

Supplementary data to this article can be found online at https://doi.org/10.1016/j.jmbbm.2022.105432.

References

Arant, B.S., 1991. Vesicoureteric reflux and renal injury. Am. J. Kidney Dis. 17, 491–511. https://doi.org/10.1016/s0272-6386(12)80490-2.

Aldaqadossi, H.A., 2013. Stone expulsion rate of small distal ureteric calculi could be predicted with plasma C-reactive protein. Urolithiasis 41, 235–239. https://doi.org/10.1007/s00240-013-0551-1.

Ahmed, A.F., Gabr, A.H., Emara, A.A., Ali, M., Abdel-Aziz, A.S., Alshahrani, S., 2015. Factors predicting the spontaneous passage of a ureteric calculus of ⩽10mm. Arab. J. Urol. 13, 84–90. https://doi.org/10.1016/j.aju.2014.11.004.

Alelign, T., Petros, B., 2018. Kidney stone disease: an update on current concepts. Adv. Urol. 1–12. https://doi.org/10.1155/2018/3068365, 2018.

Chandrasekharaiah, D.S., Debnath, L., 1994. Continuum Mechanics. Academic Press, America.

Chauhan, C.K., Joshi, M.J., Vaidya, A.D.B., 2009. Growth inhibition of struvite crystals in the presence of herbal extract Commiphora wightii. J. Mater. Sci. Mater. Med. 20, S85–S92. https://doi.org/10.1007/s10856-008-3489-z.

Chrispell, J., Fauci, L., 2011. Peristaltic pumping of solid particles immersed in a viscoelastic fluid. Math. Model Nat. Phenom. 6, 67–83. https://doi.org/10.1051/mmnp/20116504.

Cloutier, J., Villa, L., Traxer, O., Daudon, M., 2015. Kidney stone analysis: "Give me your stone, I will tell you who you are!". World. J. Urol. 33, 157–169. https://doi.org/10.1051/mmnp/20116504.

Cruz-May, T.N., Herrera, A., Rodríguez-Hernández, J., Basulto-Martínez, M., Flores-Tapia, J.P., Quintanaa, P., 2021. Structural and morphological characterization of kidney stones in patients from the Yucatan Maya population. J. Mol. Struct. 1235 (1), 130267 https://doi.org/10.1016/j.molstruc.2021.130267, 130267(10).

Goertz, J.K., Lotterman, S., 2010. Can the degree of hydronephrosis on ultrasound predict kidney stone size? Am. J. Emerg. Med. 28, 813–816. https://doi.org/10.1016/j.ajem.2009.06.028.

Hanna, M.K., Jeffs, R.D., Sturgess, J.M., Barkin, M., 1976. Ureteral structure and ultrastructure. Part I. The normal human ureter. J. Urol. 116, 718–724. https://doi.org/10.1016/S0022-5347(17)58986-7.

Hosseini, G., Ji, C., Xu, D., Rezaienia, M.A., Avital, E., Munjiza, A., Williams, J.J.R., Green, J.S.A., 2018. A computational model of ureteral peristalsis and an investigation into ureteral reflux. Biomed. Eng. Lett. 8, 117–125. https://doi.org/10.1007/s13534-017-0053-0.

Jendeberg, J., Geijer, H., Alshamari, M., Cierzniak, B., Lidén, M., 2017. Size matters:The width and location of a ureteral stone accurately predict the chance of spontaneous passage. Eur. Radiol. 27, 4775–4785. https://doi.org/10.1007/s00330-017-4852-6.

López, M., Hoppe, B., 2010. History, epidemiology and regional diversities of urolithiasis. Pediatr. Nephrol. 25, 49–59. https://doi.org/10.1007/s00467-008-0960-5.

Miller, O.F., Kane, C.J., 1999. Time to stone passage for observed ureteral calculi: a guide for patient education. J. Urol. 162, 688–691. https://doi.org/10.1097/00005392-199909010-00014.

Mokhless, I., Zahran, A.R., Youssif, M., Fouda, K., Fahmy, A., 2012. Factors that predict the spontaneous passage of ureteric stones in children. Arab. J. Urol. 10, 402–407. https://doi.org/10.1016/j.aju.2012.05.002.

Morris, R.M., Leach, P.G.L., 2015. Symmetry reductions and solutions to the Zoomeron equation. Phys. Scripta 90 (1), 015202. https://doi.org/10.1088/0031-8949/90/1/015202, 015202(5).

Ma, Y.J., Choic, J., Hourlier-Fargettec, A., Xue, Y.G., Chung, H.U., Lee, J.Y., Wang, X.F., Xie, Z.Q., Kang, D., Wang, H.L., Han, S.Y., Kang, S.K., Kang, Y., Yu, X., Slepian, M.J., Raj, M.S., Model, J.B., Feng, X., Ghaffari, R., Rogers, J.A., Huang, Y.G., 2018. Relation between blood pressure and pulse wave velocity for human arteries. P. Natl. Acad. Sci. USA. 115, 11144–11149. https://doi.org/10.1073/pnas.1814392115.

Mohammadinejad, P., Ferrero, A., Bartlett, D.J., Khandelwal, A., Marcus, R., Lieske, J.C., Moen, T.R., Mara, K.C., Enders, F.T., McCollough, C.H., Fletcher, J.G., 2021. Automated radiomic analysis of CT images to predict likelihood of spontaneous passage of symptomatic renal stones. Emerg. Radiol. 28, 781–788. https://doi.org/10.1007/s10140-021-01915-4.

Najafi, Z., Gautam, P., Schwartz, B.F., Chandy, A.J., Mahajan, A.M., 2016. Three-dimensional numerical simulations of peristaltic contractions in obstructed ureter flows. J. Biomech. Eng. 138 (1), 101002 https://doi.org/10.1115/1.4034307, 101002(7).

Özcan, C., Aydoğdu, O., Senocak, C., Damar, E., Eraslan, A., Oztuna, D., Bozkurt, O.F., 2015. Predictive factors for spontaneous stone passage and the potential role of serum C-reactive protein in patients with 4 to 10 mm distal ureteral stones: a prospective clinical study. J. Urol. 194, 1009–1013. https://doi.org/10.1016/j.juro.2015.04.104.

Preminger, G.M., Tiselius, H.G., Assimos, D.G., Alken, P., Buck, C., Gallucci, M., Knoll, T., Lingeman, J.E., Nakada, S.Y., Pearle, M.S., Sarica, K., Türk, C., Wolf, J.S., 2007. 2007 guideline for the management of ureteral calculi. J. Urol. 178, 2418–2434. https://doi.org/10.1016/j.juro.2007.09.107.

Park, C.H., Ha, J.Y., Park, C.H., Kim, C.I., Kim, K.S., Kim, B.H., 2013. Relationship between spontaneous passage rates of ureteral stones less than 8 mm and serum C-reactive protein levels and neutrophil percentages. Korean. J. Urol. 54, 615–618. https://doi.org/10.4111/kju.2013.54.9.615.

Popov, V.L., 2017. Contact Mechanics and Friction: Physical Principles and Applications, second ed. Springer Berlin Heidelberg, Berlin.

Rassoli, A., Shafigh, M., Seddighi, A., Seddighi, A., Daneshparvar, H., Fatouraee, N., 2014. Biaxial mechanical properties of human ureter under tension. Urol. J. 11, 1678–1686. https://pubmed.ncbi.nlm.nih.gov/25015616/.

Reimer, R.P., Salem, J., Merkt, M., Sonnabend, K., Lennartz, S., Zopfs, D., Heidenreich, A., Maintz, D., Haneder, S., Hokamp, N.G., 2020. Size and volume of kidney stones in computed tomography: influence of acquisition techniques and image reconstruction parameters. Eur. J. Radiol. 132 (1), 109267 https://doi.org/10.1016/j.ejrad.2020.109267, 109267(6).

Schwalb, D.M., Eshghi, M., Ian, M.D., Franco, I., 1993. Morphological and physiological changes in the urinary tract associated with ureteral dilation and ureteropyeloscopy: an experimental study. J. Urol. 149, 1576–1585. https://doi.org/10.1016/S0022-5347(17)36456-X.

Segura, J.W., Preminger, G.M., Assimos, D.G., Dretler, S.P., Kahn, R.I., Lingeman, J.E., Macaluso, J.N., 1997. Ureteral stones clinical guidelines panel summary report on the management of ureteral calculi. J. Urol. 158, 1915–1921. https://doi.org/10.1016/s0022-5347(01)64173-9.

Song, H.J., Cho, S.T., Kim, K.K., 2010. Investigation of the location of the ureteral stone and diameter of the ureter in patients with renal colic. Korean. J. Urol. 51, 198–201. https://doi.org/10.4111/kju.2010.51.3.198.

Sokolis, D.P., 2011. Multiaxial mechanical behaviour of the passive ureteral wall: experimental study and mathematical characterisation. Comput. Method. Biomec. 15, 1145–1156. https://doi.org/10.1080/10255842.2011.581237.

Sfoungaristos, S., Kavouras, A., Perimenis, P., 2012. Predictors for spontaneous stone passage in patients with renal colic secondary to ureteral calculi. Int. Urol. Nephrol. 44, 71–79. https://doi.org/10.1007/s11255-011-9971-4.

Sokolis, D.P., 2014. Identification and characterisation of regional variations in the material properties of ureter according to microstructure. Comput. Method. Biomec. 17, 1653–1670. https://doi.org/10.1080/10255842.2012.761692.

Sokolis, D.P., Petsepe, D.C., Papadodima, S.A., Kourkoulis, S.K., 2017. Age- and region-related changes in the biomechanical properties and composition of the human ureter. J. Biomech. 51, 57–64. https://doi.org/10.1016/j.jbiomech.2016.11.067.

Timoshenko, S.P., Goodier, J.N., 1970. Theory of Elasticity, third ed. McGraw-Hill, New York.

Tzortzis, V., Mamoulakis, C., Rioja, J., Gravas, S., Michel, M.C., de la Rosette, J.J.M.C.H., 2009. Medical expulsive therapy for distal ureteral stones. Drugs 69, 677–692. https://doi.org/10.2165/00003495-200969060-00003.

Takaddus, A.T., Chandy, A.J., 2018. A three-dimensional (3D) two-way coupled fluid-structure interaction (FSI) study of peristaltic flow in obstructed ureters. Int. J. Numer. Meth. Biomed. Engng. 34 (1), e3122 https://doi.org/10.1002/cnm.3122. -e3122(13).

Takaddus, A.T., Gautam, P., Chandy, A.J., 2018. A fluid-structure interaction (FSI)-based numerical investigation of peristalsis in an obstructed human ureter. Int. J. Numer. Meth. Biomed. Engng. 34 (1), e03104 https://doi.org/10.1002/cnm.3104 e03104 (13).

Ueno, A., Kawamura, T., Ogawa, A., Takayasu, H., 1977. Relation of spontaneous passage of ureteral calculi to size. Urology 10, 544–546. https://doi.org/10.1016/0090-4295(77)90097-8.

Vahidi, B., Fatouraee, N., Imanparast, A., Moghadam, A.N., 2011. A mathematical simulation of the ureter: effects of the model parameters on ureteral pressure/flow relations. J. Biomech. Eng. 133 (1), 031004 https://doi.org/10.1115/1.4003316, 031004(9).

Vahidi, B., Fatouraee, N., 2012. A biomechanical simulation of ureteral flow during peristalsis using intraluminal morphometric data. J. Theor. Biol. 298, 42–50. https://doi.org/10.1016/j.jtbi.2011.12.019.

Woodburne, R.T., Lapides, J., 1972. The ureteral lumen during peristalsis. Am. J. Anat. 133, 255–258. https://doi.org/10.1002/aja.1001330302.

Yin, F.C., Fung, Y.C., 1971. Mechanical properties of isolated mammalian ureteral segments. Am. J. Physiol. 221, 1484–1493. https://doi.org/10.1152/ajplegacy.1971.221.5.1484.

Yankelevsky, D.Z., Eisenberger, M., 1986. Analysis of a beam column on elastic foundation. Comput. Struct. 23, 351–356. https://doi.org/10.1016/0045-7949(86)90226-9.

Yoshida, T., Inoue, T., Omurac, N., Okada, S., Hamamoto, S., Kinoshita, H., Matsuda, T., 2017. Ureteral wall thickness as a preoperative indicator of impacted stones in patients with ureteral stones undergoing ureteroscopic lithotripsy. Urology 106, 45–49. https://doi.org/10.1016/j.urology.2017.04.047.

Zhong, P., Chuong, C.J., Preminger, G.M., 1993. Characterization of fracture toughness of renal calculi using a microindentation technique. J. Mater. Sci. Lett. 12, 1460–1462. https://doi.org/10.1007/BF00591608.

Zhang, L.T., Steinberg, P.L., 2019. Kidney stone removal procedures and emerging therapies. In: Han, H., Mutter, W.P., Nasser, S. (Eds.), Nutritional and Medical Management of Kidney Stones. Humana, Cham, pp. 83–90.

Zhu, W.J., Ma, M.M., Zheng, M.M., Hao, H., Yang, K.L., Zhou, L.Q., Zhang, J.S., Wang, H., Li, X.S., 2020. Cine magnetic resonance urography for postoperative evaluation of reconstructive urinary tract after ileal ureter substitution: initial experience. Clin. Radiol. 75 https://doi.org/10.1016/j.crad.2020.01.014, 480.e1-480.e9.